Polar Coordinate Representation of $H_b(r_c)$ versus $(\hbar^2/8m)\nabla^2\rho_b(r_c)$ at BCP in AIM Analysis: Classification and Evaluation of Weak to Strong Interactions

Waro Nakanishi,* Satoko Hayashi, and Kenji Narahara

Department of Material Science and Chemistry, Faculty of Systems Engineering, Wakayama University, 930 Sakaedani, Wakayama, 640-8510 Japan

Received: April 20, 2009; Revised Manuscript Received: June 13, 2009

Polar coordinate (R, θ) representation is proposed for the plot of $H_b(\boldsymbol{r}_c)$ versus $(\hbar^2/8m)\nabla^2\rho_b(\boldsymbol{r}_c)$ in AIM analysis to classify, evaluate, and understand weak to strong interactions in a unified way and in more detail; $H_b(\boldsymbol{r}_c)$ and $\nabla^2\rho_b(\boldsymbol{r}_c)$ are total electron energy densities and the Laplacian of $\rho_b(\boldsymbol{r}_c)$ at bond critical points (BCPs: $\boldsymbol{r}_c$), respectively, where $\rho_b(\boldsymbol{r}_c)$ are electron densities at $\boldsymbol{r}_c$. Both the *x*- and *y*-axes of the plot are expressed in the common unit of energy since $H_b(\boldsymbol{r}_c) = G_b(\boldsymbol{r}_c) + V_b(\boldsymbol{r}_c)$ and $(\hbar^2/8m)\nabla^2\rho_b(\boldsymbol{r}_c) = H_b(\boldsymbol{r}_c) - V_b(\boldsymbol{r}_c)/2$ $(= G_b(\boldsymbol{r}_c) + V_b(\boldsymbol{r}_c)/2)$, where $G_b(\boldsymbol{r}_c)$ and $V_b(\boldsymbol{r}_c)$ are kinetic energy densities and potential energy densities, respectively. Data employed for the plot are calculated at BCPs for full-optimized structures and optimized structures with the fixed distances (r) of $r = r_o + wa_o$, where r_o are the full-optimized distances, a_o is the Bohr radius, and $w = \pm 0.1$ and ± 0.2. The plot draws a helical stream starting from near origin $(H_b(\boldsymbol{r}_c) = (\hbar^2/8m)\nabla^2\rho_b(\boldsymbol{r}_c) = 0)$ for very weak interactions and turns to the right as interactions become stronger. The helical stream is well described by the polar coordinate representation with (R, θ); R is given in the energy unit, and θ in degrees is measured from the *y*-axis. The ratio of $V_b(\boldsymbol{r}_c)/G_b(\boldsymbol{r}_c)$ $(= k)$ controls θ, of which an acceptable range in the plot is $45.0 < \theta < 206.6°$. Each plot for an interaction gives a curve, which supplies important information. It is expressed by θ_p and κ_p; θ_p corresponds to the tangent line measured from the *y*-direction, and κ_p is the curvature of the plot at $w = 0$. The polar coordinate (R, θ) representation with (θ_p, κ_p) helps us to classify, evaluate, and understand the nature of weak to strong interactions in a unified way.

Introduction

The atoms-in-molecules method (AIM)[1,2] enables us to analyze the nature of chemical bonds and interactions.[3−8] Electron densities at bond critical points (BCPs: $\boldsymbol{r}_c$, *) $(\rho_b(\boldsymbol{r}_c))$ and the Laplacian of $\rho_b(\boldsymbol{r}_c)$ $(\nabla^2\rho_b(\boldsymbol{r}_c))$ can be evaluated experimentally.[1] The $\rho_b(\boldsymbol{r}_c)$ are strongly related to the binding energies[9−16] and bond orders (BO).[17] The sign of $\nabla^2\rho_b(\boldsymbol{r}_c)$ indicates that $\rho_b(\boldsymbol{r}_c)$ is depleted or concentrated with respect to the surroundings since $\nabla^2\rho_b(\boldsymbol{r}_c)$ is the second derivative of $\rho_b(\boldsymbol{r}_c)$. The $\rho_b(\boldsymbol{r}_c)$ is locally depleted relative to the average distribution around $\boldsymbol{r}_c$ if $\nabla^2\rho_b(\boldsymbol{r}_c) > 0$, but it is concentrated when $\nabla^2\rho_b(\boldsymbol{r}_c) < 0$. Total electron energy densities at BCPs $(H_b(\boldsymbol{r}_c))$ would be a more appropriate index for weak interactions on the energy basis.[1,18] $H_b(\boldsymbol{r}_c)$ are the sum of kinetic energy densities $(G_b(\boldsymbol{r}_c))$ and potential energy densities $(V_b(\boldsymbol{r}_c))$ at BCPs, as shown in eq 1. Equation 2 represents the relation between $H_b(\boldsymbol{r}_c)$ and $\nabla^2\rho_b(\boldsymbol{r}_c)$.

$$H_b(\boldsymbol{r}_c) = G_b(\boldsymbol{r}_c) + V_b(\boldsymbol{r}_c) \tag{1}$$

$$(\hbar^2/8m)\nabla^2\rho_b(\boldsymbol{r}_c) = H_b(\boldsymbol{r}_c) - V_b(\boldsymbol{r}_c)/2 \tag{2}$$

$$= G_b(\boldsymbol{r}_c) + V_b(\boldsymbol{r}_c)/2 \tag{2'}$$

Scheme 1 summarizes the role of $\nabla^2\rho_b(\boldsymbol{r}_c)$ and $H_b(\boldsymbol{r}_c)$ to classify the interactions. Interactions in the region of $\nabla^2\rho_b(\boldsymbol{r}_c) < 0$ are called shared-shell (SS) interactions, and they are closed-shell (CS) interactions for $\nabla^2\rho_b(\boldsymbol{r}_c) > 0$. Interactions exhibit the covalent nature when $H_b(\boldsymbol{r}_c) < 0$ since electrons at BCPs are stabilized in the region, whereas they exhibit no covalency if $H_b(\boldsymbol{r}_c) > 0$ due to the destabilization of electrons at BCPs under the conditions. $H_b(\boldsymbol{r}_c)$ must be negative when $\nabla^2\rho_b(\boldsymbol{r}_c) < 0$ since $H_b(\boldsymbol{r}_c)$ are larger than $(\hbar^2/8m)\nabla^2\rho_b(\boldsymbol{r}_c)$ by $V_b(\boldsymbol{r}_c)/2$, where $V_b(\boldsymbol{r}_c)$ are negative at all BCPs (eq 2). Consequently, $\nabla^2\rho_b(\boldsymbol{r}_c) < 0$ and $H_b(\boldsymbol{r}_c) < 0$ for the SS interactions. The CS interactions are especially called pure CS interactions for $H_b(\boldsymbol{r}_c) > 0$ and $\nabla^2\rho_b(\boldsymbol{r}_c) > 0$ since electrons at BCPs are depleted and destabilized under the conditions.[13a] Electrons in the intermediate region between SS and pure CS, which belong to CS, are locally depleted but stabilized at BCPs since $\nabla^2\rho_b(\boldsymbol{r}_c) > 0$ but $H_b(\boldsymbol{r}_c) < 0$.[13a] The redistribution of $\rho_b(\boldsymbol{r}_c)$ occurs between those electronic states in this region.

SCHEME 1: Shared-Shell and Closed-Shell Interactions Related to $\nabla^2\rho_b(\boldsymbol{r}_c)$ and $H_b(\boldsymbol{r}_c)$

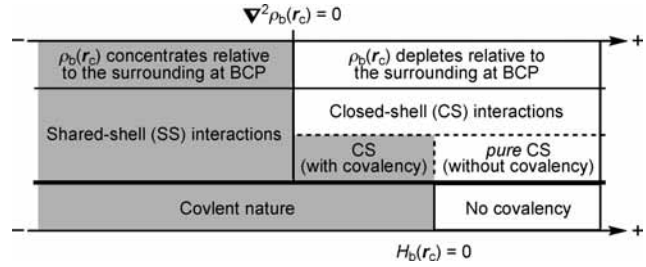

We have paid much attention to weak interactions[19−28] since they determine fine structures of compounds and create high functionalities of materials. They play an important role in physical, chemical, and biological sciences.[29−33] It is of high importance to clarify the cause-and-effect in the phenomena

* To whom correspondence should be addressed. Tel: +81 73 457 8252. Fax: +81 73 457 8253. E-mail: nakanisi@sys.wakayama-u.ac.jp.

10.1021/jp903622a CCC: $40.75
Published on Web 07/21/2009

SCHEME 2: Interactions Examined in This Work[a]

vdW	HB
HeHF (He-∗-H)	NNHF (N-∗-H)
NeHF (Ne-∗-H)	HFHF (F-∗-H)
ArHF (Ar-∗-H)	HCNHF (N-∗-H)
KrHF (Kr-∗-H)	H_2OHOH (O-∗-H)
	Me_2OHOH (O-∗-H)
CT-MC	**X_3^- & CT-TBP**
Me_2OCl_2 (MC) (O-∗-Cl)	Cl_3^- (Cl-∗-ClCl)
Me_2OBr_2 (MC) (O-∗-Br)	$BrCl_2^-$ (Cl-∗-BrCl)
Me_2SCl_2 (MC) (S-∗-Cl)	Br_3^- (Br-∗-BrBr)
Me_2SBr_2 (MC) (S-∗-Br)	$ClBr_2^-$ (Br-∗-ClBr)
Me_2SeCl_2 (MC) (Se-∗-Cl)	Me_2SCl_2 (TBP) (S-∗-Cl)
Me_2SeBr_2 (MC) (Se-∗-Br)	Me_2SBr_2 (TBP) (S-∗-Br)
	Me_2SeCl_2 (TBP) (Se-∗-Cl)
	Me_2SeBr_2 (TBP) (Se-∗-Br)
Cov-w	**Cov-s**
Cl_2 (Cl-∗-Cl)	H_2 (H-∗-H)
Br_2 (Br-∗-Br)	CH_4 (C-∗-H)
Me_2SCl^+ (S-∗-Cl)	C_2H_6 (C-∗-C)
Me_2SBr^+ (S-∗-Br)	C_2H_4 (C-∗-C)
Me_2SeCl^+ (Se-∗-Cl)	C_2H_2 (C-∗-C)
Me_2SeBr^+ (Se-∗-Br)	

[a] BCPs are described by —∗—. Marks and colors are used commonly in the plots.

SCHEME 3: Bond Critical Points (BCPs: r_c, *) on the X−Y Bond[a]

Bond critical points (BCPs, r_c, ∗)

X–∗–Y

r(X, Y)

$r(X, Y) = r_o(X, Y) + wa_o$ (w = 0, ±0.1, ±0.2)

[a] The r(X, Y) are the fixed values for further optimizations, where r_o(X, Y) and a_o are the full-optimized distances and the Bohr radius, respectively.

arising from weak interactions, with physical necessity. Very recently, we reported that the characteristic helical behavior appeared in the plot of $H_b(\boldsymbol{r}_c)$ versus $\nabla^2\rho_b(\boldsymbol{r}_c)$.[34] The method must contain the high possibility to classify, evaluate, and understand weak to strong interactions in a unified form. To improve the method for the better understanding of interactions, we came to a conclusion that $H_b(\boldsymbol{r}_c)$ should be plotted versus $(\hbar^2/8m)\nabla^2\rho_b(\boldsymbol{r}_c)$ since both x- and y-axes in the plot can be expressed in the same energy unit as shown in eq 2.

We propose the polar coordinate representation with (R, θ) for the plot of $H_b(\boldsymbol{r}_c)$ versus $(\hbar^2/8m)\nabla^2\rho_b(\boldsymbol{r}_c)$. Any distances on the ($x$, y) plane of the plot are given in the energy unit since the x- and y-axes of the plot are given in the energy unit. R in (R, θ) corresponds to the energy for an interaction at the BCP in the ($H_b(\boldsymbol{r}_c) - V_b(\boldsymbol{r}_c)/2$, $H_b(\boldsymbol{r}_c)$) plane relative to that without interaction (corresponding to the origin) (see eq 5), and θ measured from the y-axis controls the helical figure of the plot. Each plot shows a specific curve if data at BCP for a full-optimized structure and those near it are plotted (see Figure 3). The curve must also be important to understand the nature of the interaction. The curve is expressed by θ_p and κ_p; θ_p corresponds to the tangent line measured from the y-direction, and κ_p is the curvature of the plot at the BCP at the full-optimized structure.

Scheme 2 shows weak to strong interactions examined in this work;[35] these include van der Waals interactions (vdW),[36] hydrogen bonds (HB),[11,37] molecular complexes through charge transfer (CT-MC), and hypervalent adducts through CT of the X_3^- (trihalide ions) and CT-TBP (trigonal bipyramidal adducts) types. Some classical covalent bonds of weak (Cov-w) and strong ones (Cov-s) are also examined. Marks with colors in Scheme 2 correspond to those in the plots. BCPs are described by —∗—. Methyl derivatives are mainly employed here since the AIM data must be close to those of usual compounds relative to the case of the parent hydrogen derivatives.[34]

Here, we propose a method to classify, evaluate, and understand weak to strong interactions in a unified way in more detail by plotting $H_b(\boldsymbol{r}_c)$ versus $(\hbar^2/8m)\nabla^2\rho_b(\boldsymbol{r}_c)$. $H_b(\boldsymbol{r}_c) - V_b(\boldsymbol{r}_c)/2$ will be often used in place of $(\hbar^2/8m)\nabla^2\rho_b(\boldsymbol{r}_c)$ without notice since $(\hbar^2/8m)\nabla^2\rho_b(\boldsymbol{r}_c) = H_b(\boldsymbol{r}_c) - V_b(\boldsymbol{r}_c)/2$. The polar coordinate ($R$, θ) representation is employed for the plot. The (θ_p, κ_p) parameters are also used to specify the curvature of each correlation. R is given in the energy unit, κ_p in the reciprocal energy unit, and θ and θ_p by degrees measured from the y-axis and y-direction, respectively. Indeed, the plot of $G_b(\boldsymbol{r}_c) + V_b(\boldsymbol{r}_c)$ versus $G_b(\boldsymbol{r}_c) + V_b(\boldsymbol{r}_c)/2$ is the synonymous representation to that of $H_b(\boldsymbol{r}_c)$ versus $H_b(\boldsymbol{r}_c) - V_b(\boldsymbol{r}_c)/2$, as shown in eq 2′, but we will employ the latter since it seems easier to image the summary shown in Scheme 1. Weak to strong interactions will be well analyzed by the treatment.

Methodological Details

Species in Scheme 2 are optimized employing the 6-311+G(3d,2p) basis sets for C and H and the 6-311+G(3df) basis sets of the Gaussian 03 program for atoms other than C and H, unless otherwise noted.[38] The 6-311++G(3df,3pd) basis sets are applied to C and H when hydrocarbons are calculated. The Møller−Plesset second-order energy correlation (MP2) level is employed for the calculations.[39]

The full-optimized X−Y length in question is given by r_o(X, Y) (= r_o). Optimizations are further performed with the fixed X−Y lengths r(X, Y) (= r) around r_o to elucidate the trend of the interaction more clearly.[40,41] The fixed lengths are given by $r(X, Y) = r_o(X, Y) + wa_o$, where a_o is the Bohr radii.[42] Data with w = 0, ±0.1, and ±0.2 are employed for usual cases. Scheme 3 explains BCPs ($\boldsymbol{r}_c$, *) and r(X, Y) employed in the calculations.[41,43] AIM parameters are calculated with the Gaussian 03 program[38] and analyzed by the AIM2000 program.[44]

Results and Discussion

Table 1 collects the values for AIM functions [$\rho_b(\boldsymbol{r}_c)$, $(\hbar^2/8m)\nabla^2\rho_b(\boldsymbol{r}_c)$ (= $H_b(\boldsymbol{r}_c) - V_b(\boldsymbol{r}_c)/2$), $H_b(\boldsymbol{r}_c)$, $G_b(\boldsymbol{r}_c)$, and $V_b(\boldsymbol{r}_c)$] and AIM parameters [k (= $V_b(\boldsymbol{r}_c)/G_b(\boldsymbol{r}_c)$), R, θ, θ_p, and κ_p] calculated at the MP2 level, together with r_o(X, Y) for various interactions in Scheme 2. Data at BCPs of the five structures with $r = r_o + wa_o$ (w = 0, ±0.1, and ±0.2) are employed for each plot, and they are used to evaluate the AIM parameters.

Before discussion of the interactions in Scheme 2, it should be instructive to explain the behaviors of the AIM parameters proposed in this work. The pre-explanation will show how the values are correlated to the interactions. Trihalide ions (X_3^-, X = Cl and Br) are employed for the pre-explanation since X_3^- can be successfully calculated under very long $[^1X\text{----}^2X\text{—}^3X]^-$ and short $[^1X\text{—}^2X\text{---}^3X]^-$ distances of $r(^1X, ^2X)$ at the singlet state. Data for Cl_3^- and Br_3^- are calculated under a very wide range of w ($-1.2 \le w \le 10.0$) in $r = r_o + wa_o$. Selected data for Cl_3^- and Br_3^- are collected in Table S1 of the Supporting Information.

AIM Parameters in Polar Coordinate Representation of $H_b(\boldsymbol{r}_c)$ versus $(\hbar^2/8m)\nabla^2\rho_b(\boldsymbol{r}_c)$. The plot of $H_b(\boldsymbol{r}_c)$ versus $(\hbar^2/8m)\nabla^2\rho_b(\boldsymbol{r}_c)$ (= $H_b(\boldsymbol{r}_c) - V_b(\boldsymbol{r}_c)/2$) is represented by the polar coordinate with (R, θ). Relations between the polar coordinate system (R, θ) and the Cartesian axes system ($H_b(\boldsymbol{r}_c) - V_b(\boldsymbol{r}_c)/2$,

TABLE 1: AIM Functions and Parameters Evaluated for van der Waals Interactions (vdW), Hydrogen Bonds (HB), Molecular Complexes (CT-MC), Trihalide Ions (X_3^-), Chalcogenide Dihalides of Trigonal Bipyramidal Structures (CT-TBP), Weak Covalent Bonds (Cov-w), and Strong Covalent Bonds (Cov-s) Calculated at the MP2 Level[a]

species (X−*−Y)	r_o(X, Y) (Å)	$\rho_b(\boldsymbol{r}_c)$ (ea_o^{-3})	$c\nabla^2\rho_b(\boldsymbol{r}_c)^b$ (au)	$H_b(\boldsymbol{r}_c)$ (au)	$G_b(\boldsymbol{r}_c)$ (au)	$V_b(\boldsymbol{r}_c)$ (au)	k^c	R (au)	θ (°)	θ_p (°)	κ_p (au^{-1})	comment
He−*−HF[d]	2.2454	0.0034	0.0022	0.0013	0.0031	−0.0018	−0.591	0.0025	59.9	57.2	8.50	vdW
Ne−*−HF[d]	2.1982	0.0076	0.0050	0.0019	0.0082	−0.0062	−0.765	0.0054	69.2	84.3	85.37	vdW
Ar−*−HF[d,e]	2.5142	0.0083	0.0043	0.0020	0.0066	−0.0046	−0.696	0.0048	65.0	76.4	162.97	vdW
Kr−*−HF[d,e]	2.6423	0.0086	0.0040	0.0017	0.0062	−0.0045	−0.722	0.0043	66.5	80.4	220.94	vdW
NN−*−HF[d]	2.0293	0.0190	0.0087	0.0015	0.0159	−0.0143	−0.903	0.0088	80.0	126.8	236.37	HB
HF−*−HF[d]	1.8196	0.0250	0.0125	−0.0002	0.0252	−0.0254	−1.007	0.0125	90.8	128.3	108.51	HB
HCN−*−HF[d]	1.8238	0.0337	0.0107	−0.0053	0.0267	−0.0320	−1.197	0.0120	116.1	168.6	24.21	HB
H_2O−*−HOH	1.9427	0.0244	0.0106	0.0005	0.0208	−0.0203	−0.976	0.0107	87.3	123.8	156.35	HB
Me_2O−*−HOH	1.8636	0.0313	0.0121	−0.0021	0.0263	−0.0284	−1.079	0.0123	99.8	148.2	87.70	HB
Me_2O−*−Cl_2	2.5513	0.0285	0.0128	0.0007	0.0248	−0.0241	−0.971	0.0128	86.8	96.4	30.91	CT-MC
Me_2O−*−Br_2	2.5913	0.0308	0.0123	−0.0004	0.0250	−0.0254	−1.015	0.0123	91.8	106.6	49.64	CT-MC
Me_2S−*−Cl_2	2.6331	0.0459	0.0108	−0.0057	0.0273	−0.0330	−1.207	0.0122	117.6	163.4	52.73	CT-MC
Me_2S−*−Br_2	2.6923	0.0477	0.0093	−0.0078	0.0265	−0.0343	−1.296	0.0122	130.0	169.9	40.53	CT-MC
Me_2Se−*−Cl_2	2.5700	0.0597	0.0093	−0.0125	0.0312	−0.0437	−1.402	0.0156	143.3	181.5	9.13	CT-MC
Me_2Se−*−Br_2	2.7286	0.0510	0.0078	−0.0102	0.0257	−0.0359	−1.396	0.0128	142.7	180.1	13.49	CT-MC
$[Cl-*-Cl_2]^-$[d]	2.2956	0.0836	0.0133	−0.0220	0.0485	−0.0705	−1.454	0.0257	149.0	181.6	10.96	X_3^-
$[Br-*-Br_2]^-$[d]	2.5474	0.0678	0.0078	−0.0185	0.0341	−0.0526	−1.543	0.0201	157.2	183.8	7.38	X_3^-
$[Cl-*-BrCl]^-$[d]	2.4022	0.0763	0.0100	−0.0225	0.0424	−0.0649	−1.530	0.0246	156.1	182.9	6.21	X_3^-
$[Br-*-ClBr]^-$[d]	2.4392	0.0728	0.0104	−0.0182	0.0390	−0.0572	−1.465	0.0210	150.1	181.3	11.98	X_3^-
Me_2ClS−*−Cl	2.2650	0.0967	0.0046	−0.0364	0.0457	−0.0821	−1.798	0.0367	172.8	191.7	5.31	CT-TBP
Me_2BrS−*−Br	2.4387	0.0810	0.0048	−0.0258	0.0354	−0.0613	−1.728	0.0262	169.4	188.5	8.31	CT-TBP
Me_2ClSe−*−Cl	2.3547	0.0869	0.0053	−0.0335	0.0441	−0.0776	−1.759	0.0339	171.0	184.0	0.66	CT-TBP
Me_2BrSe−*−Br	2.5196	0.0758	0.0035	−0.0262	0.0333	−0.0594	−1.787	0.0264	172.3	186.6	1.74	CT-TBP
Me_2S^+−*−Cl	1.9791	0.1714	−0.0241	−0.1197	0.0716	−0.1913	−2.673	0.1221	191.4	198.2	0.03	Cov-w
Me_2S^+−*−Br	2.1433	0.1402	−0.0110	−0.0798	0.0579	−0.1377	−2.380	0.0806	187.8	193.8	0.32	Cov-w
Me_2Se^+−*−Cl	2.1089	0.1397	−0.0070	−0.0849	0.0710	−0.1559	−2.197	0.0852	184.7	185.6	1.03	Cov-w
Me_2Se^+−*−Br	2.2636	0.1207	−0.0075	−0.0636	0.0486	−0.1121	−2.308	0.0640	186.7	190.1	0.37	Cov-w
Cl−*−Cl[d]	1.9845	0.1641	−0.0087	−0.0985	0.0811	−0.1796	−2.213	0.0988	185.0	194.2	0.62	Cov-w
Br−*−Br[d]	2.2690	0.1171	−0.0040	−0.0586	0.0506	−0.1093	−2.158	0.0588	183.9	190.4	0.24	Cov-w
HC−*−CH[f]	1.2107	0.4077	−0.1529	−0.6048	0.2990	−0.9039	−3.022	0.6238	194.2	196.1	0.04	Cov-s
H_2C−*−CH_2[f]	1.3349	0.3485	−0.1335	−0.4195	0.1524	−0.5718	−3.754	0.4402	197.7	199.7	0.002	Cov-s
H_3C−*−CH_3[d,f]	1.5236	0.2444	−0.0718	−0.2097	0.0661	−0.2758	−4.170	0.2216	198.9	201.1	0.07	Cov-s
H_3C−*−H[f]	1.0854	0.2821	−0.1265	−0.3075	0.0546	−0.3622	−6.631	0.3325	202.4	202.3	0.12	Cov-s
H−*−H[f]	0.7366	0.2733	−0.1544	−0.3154	0.0065	−0.3220	−49.261	0.3512	206.1	206.4	0.01	Cov-s

[a] The 6-311+G(3d,2p) basis sets being employed for C and H and the 6-311+G(3df) basis sets for atoms other than C and H. [b] $c = \hbar^2/8m$. [c] $k = V_b(\boldsymbol{r}_c)/G_b(\boldsymbol{r}_c)$. [d] See also ref 34. [e] The 6-311G(3df) basis sets being employed for Ar and Kr. [f] The 6-311+G(3df,3pd) basis sets being employed for C and H.

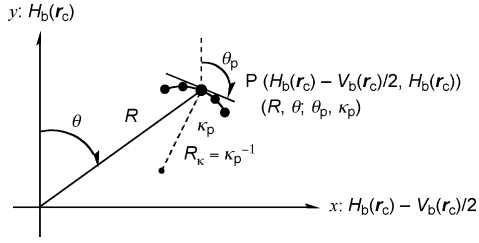

Figure 1. Polar coordinate representation of $H_b(\boldsymbol{r}_c)$ versus $H_b(\boldsymbol{r}_c) - V_b(\boldsymbol{r}_c)/2$.

$H_b(\boldsymbol{r}_c)$) are given by eqs 3−8.[45] R is given in the energy unit (au) and θ in the degree unit (°) measured from the y-axis. Each plot shows a specific curve, which is expressed by the (θ_p, κ_p) parameters. Relations for θ_p and κ_p are given in eqs 9 and 10, respectively, where x and y stand for $H_b(\boldsymbol{r}_c) - V_b(\boldsymbol{r}_c)/2$ and $H_b(\boldsymbol{r}_c)$, respectively. θ_p is the tangent line measured from the y-direction, and κ_p is the curvature of the plot. θ_p and κ_p are given in degrees and au^{-1}, respectively. The radius of curvature R_κ is given by $R_\kappa = \kappa_p^{-1}$. Figure 1 shows the proposed polar coordinate system.

$$H_b(\boldsymbol{r}_c) - V_b(\boldsymbol{r}_c)/2 = R \sin\theta \tag{3}$$

$$H_b(\boldsymbol{r}_c) = R \cos\theta \tag{4}$$

$$R = [(H_b(\boldsymbol{r}_c) - V_b(\boldsymbol{r}_c)/2)^2 + H_b(\boldsymbol{r}_c)^2]^{1/2} \tag{5}$$

$$= [2(G_b(\boldsymbol{r}_c) + 3V_b(\boldsymbol{r}_c)/4)^2 + V_b(\boldsymbol{r}_c)^2/8]^{1/2} \quad \text{(cf. eq 1)} \tag{6}$$

$$= G_b(\boldsymbol{r}_c)[5/4(k + 6/5)^2 + 1/5]^{1/2} \quad (V_b(\boldsymbol{r}_c) = kG_b(\boldsymbol{r}_c)) \tag{7}$$

$$\theta = 90° - \tan^{-1}\alpha \quad (\alpha = 2(k + 1)/(k + 2) \text{ in } H_b(\boldsymbol{r}_c) = \alpha[H_b(\boldsymbol{r}_c) - V_b(\boldsymbol{r}_c)/2]) \tag{8}$$

$$\theta_p = 90° - \tan^{-1}(dy/dx) \tag{9}$$

$$\kappa_p = |d^2y/dx^2|/[1 + (d^2y/dx)^2]^{3/2} \quad (x = H_b(\boldsymbol{r}_c) - V_b(\boldsymbol{r}_c)/2 \text{ and } y = H_b(\boldsymbol{r}_c) \text{ for eqs 9 and 10}) \tag{10}$$

Behaviors of AIM Parameters in a Helical Stream. Figure 2 shows the plots of $H_b(\boldsymbol{r}_c)$ versus $H_b(\boldsymbol{r}_c) - V_b(\boldsymbol{r}_c)/2$ for Cl_3^- and Br_3^-. Panel (a) in Figure 2 shows the whole picture and

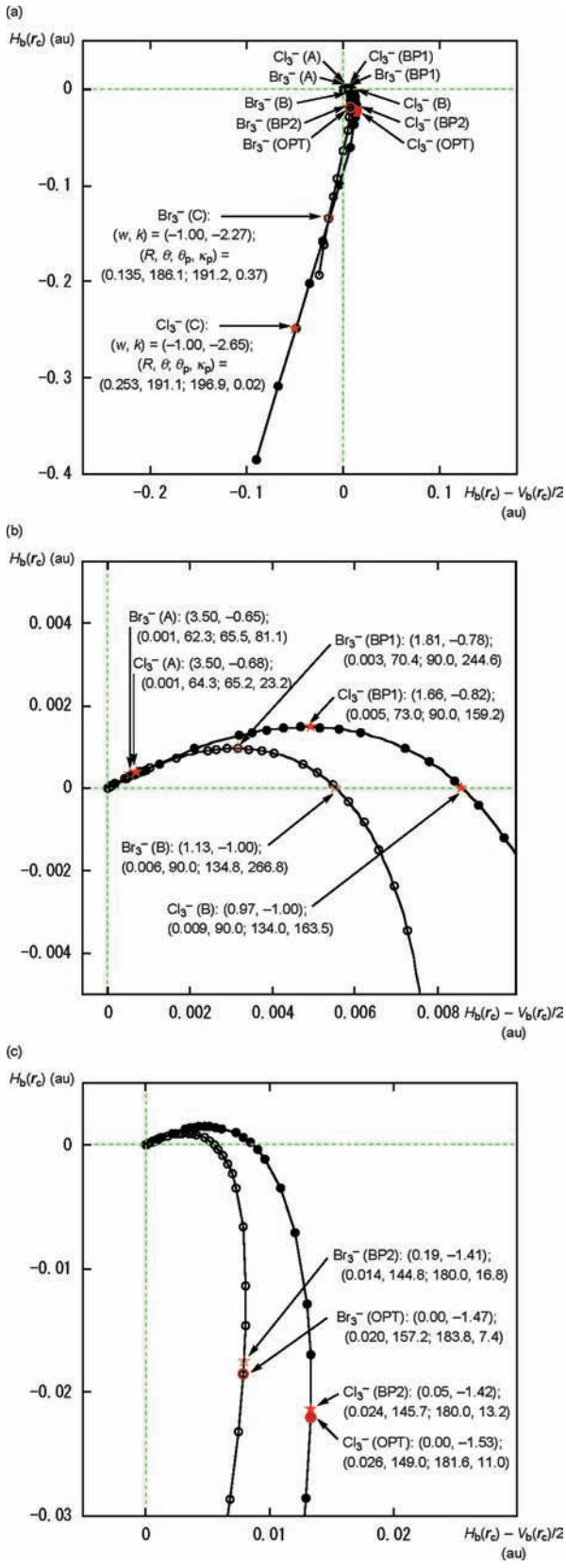

Figure 2. Plots of $H_b(r_c)$ versus $H_b(r_c) - V_b(r_c)/2$ for Cl_3^- (●) and Br_3^- (○); (a) whole picture of the plots, (b) partial ones around the origin, and (c) those around the full-optimized structures. Red circles correspond to the data at the full-optimized structures. AIM parameters of (w, k) and (R, θ; θ_p, κ_p) for Cl_3^- and Br_3^- at BP1, BP2, OPT (full-optimized structures; $w = 0.0$), A ($w = 3.5$), B (x-intercepts; $H_b(r_c) = 0$), and C ($w = 1.0$) are drawn in the figure with stars.

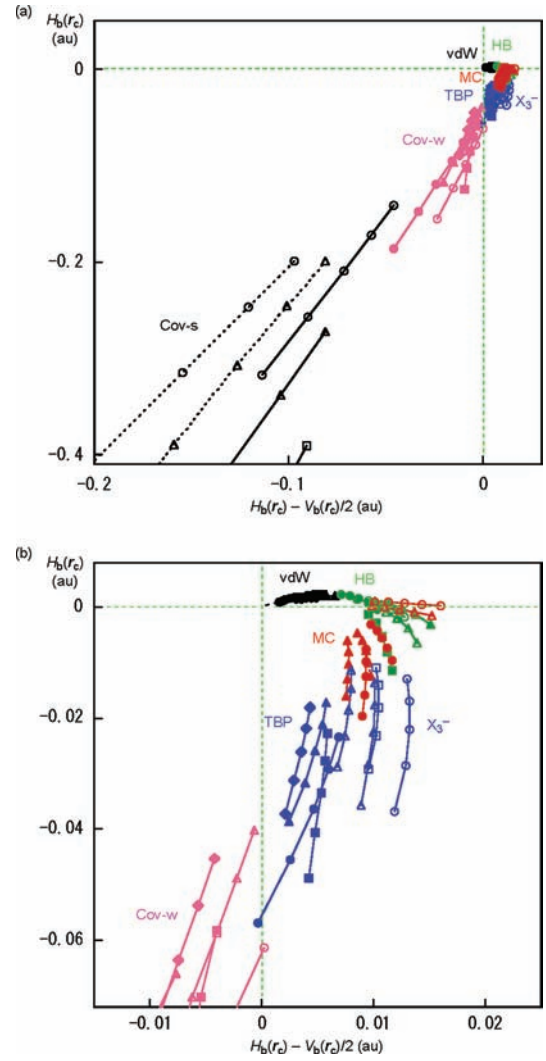

Figure 3. Plots of $H_b(r_c)$ versus $H_b(r_c) - V_b(r_c)/2$ for the species in Scheme 2 calculated at $r = r_o + wa_o$ ($w = 0$, ±0.1, and ±0.2); (a) whole picture of the plots and (b) the partial one for vdW, HB, CT-MC, X_3^-, CT-TBP, and some Cov-w interactions.

panels (b) and (c) in the figure exhibit the partial pictures around the origin and the full-optimized structures, respectively. The x- and y-axes in panel (a) are drawn to the same magnitude to build the real image for the plot. The plots of $H_b(r_c)$ and $H_b(r_c) - V_b(r_c)/2$ versus w in $r(^1X, ^2X) = r_o(^1X, ^2X) + wa_o$ for $^1X-^2X-^3X^-$ (X = Cl and Br) are shown in Figure S1 of the Supporting Information.

The $H_b(r_c)$ and $H_b(r_c) - V_b(r_c)/2$ values change largely in the plots since a very wide range of w ($-1.2 \le w \le 10.0$) in $r = r_o + wa_o$ is employed in the plots.[43] The correlation lines in Figure 2 would correspond to mean helical curves for some kinds of interactions.[34] The first bending points (BP1) for Cl_3^- and Br_3^- appear when $H_b(r_c)$ are largest ($dy/dx = 0$), and the second bending points (BP2) appear when $H_b(r_c) - V_b(r_c)/2$ are largest ($1/(dy/dx) = 0$).

Figure 2 contains the AIM parameters (R, θ; θ_p, κ_p) with (w, k) for Cl_3^- and Br_3^- at BP1, BP2, OPT (full-optimized structures; $w = 0.0$), A (point A; near origin; $w = 3.5$), B (x-intercepts; $H_b(r_c) = 0$), and C ($w = -1.0$). Interactions at C are classified as Cov-s for Cl_3^- and Cov-w for Br_3^-. The R, θ, and θ_p values become larger monotonically as k increases, and κ_p are very large at around BP1 and B.

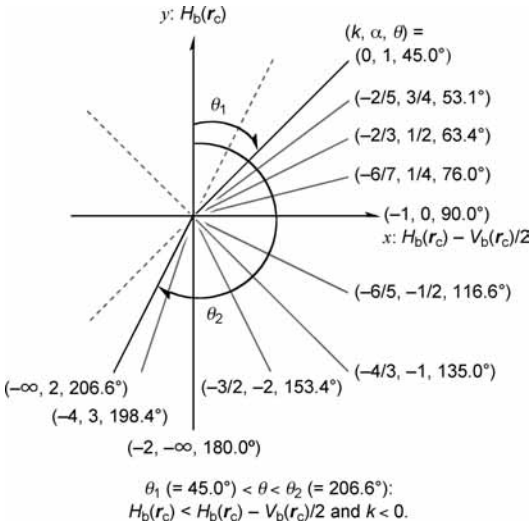

Figure 4. Acceptable range of θ in the plots of $H_b(\boldsymbol{r}_c)$ versus $H_b(\boldsymbol{r}_c) - V_b(\boldsymbol{r}_c)/2$.

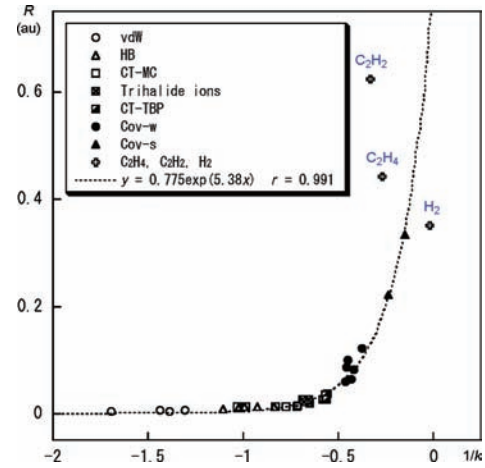

Figure 5. Plot of R versus $1/k$. The dotted line corresponds to the correlation for CT-MC, X_3^-, CT-YBP, Cov-w, and Cov-s, except for $Me_2O\cdots X_2$ (MC, X = Cl and Br), H_2, C_2H_4, and C_2H_2.

After pre-explanation of the behaviors of the AIM functions exemplified by Cl_3^- and Br_3^-, the next extension is to discuss the parameters for usual species shown in Scheme 2.

AIM Dual Functional Analysis of Weak to Strong Interactions. Figure 3 shows the plots of $H_b(\boldsymbol{r}_c)$ versus $H_b(\boldsymbol{r}_c) - V_b(\boldsymbol{r}_c)/2$ for weak to strong interactions for the species shown in Scheme 2.

Data at BCPs for the full-optimized and partially optimized structures with the fixed values ($r = r_o + wa_o$; $w = 0.0$, ±0.1, and ±0.2) are employed for the plots. Panels (a) and (b) in Figure 3 exhibit the whole picture and the partial one for vdW, HB, CT-MC, X_3^-, and CT-TBP with some Cov-w, respectively. The x-axis of Figure 3 is drawn to twice the scale relative to that for the y-axis, which enables us to realize the helical stream more visually. Data calculated at $r = r_o + wa_o$ ($w = \pm0.1$ and ±0.2) behave similarly to those at $r = r_o$ in the plots. The plots show a helical figure as a whole.[34] Plots bend around the border area between vdW and HB (BP1) and the area around X_3^- (BP2). Each plot gives the specific curvature; the curvature is represented by the (θ_p, κ_p) parameters, which are given in Table 1.

Coverage in Plots of $H_b(\boldsymbol{r}_c)$ versus $H_b(\boldsymbol{r}_c) - V_b(\boldsymbol{r}_c)/2$. The coverage in the plots of $H_b(\boldsymbol{r}_c)$ versus $H_b(\boldsymbol{r}_c) - V_b(\boldsymbol{r}_c)/2$ must be closely related to the acceptable range of θ in the plots. The θ value is controlled by k ($= V_b(\boldsymbol{r}_c)/G_b(\boldsymbol{r}_c)$) via α as shown in eq 8. The k value must be negative since $V_b(\boldsymbol{r}_c) < 0$ and $G_b(\boldsymbol{r}_c) > 0$. This requirement restricts the range of α ($= 2(k + 1)/(k + 2)$) to be $\alpha < 1.0$ or $\alpha > 2.0$; $\alpha = 1.0$ ($k = 0$) corresponds to $\theta = 45.0°$ ($= \theta_1$) in the first quadrant and $\alpha = 2.0$ ($k = -\infty$) to $\theta = 206.6°$ ($= \theta_2$) in the third quadrant. The line of $\theta = \theta_1$ ($= 45.0°$) in the first quadrant must be the asymptotic line of the plots for very weak interactions and that of $\theta = \theta_2$ ($= 206.6°$) in the third quadrant is for very strong interactions. In addition, $H_b(\boldsymbol{r}_c)$ must be smaller than $H_b(\boldsymbol{r}_c) - V_b(\boldsymbol{r}_c)/2$. Therefore, θ must be larger than θ_1 ($= 45.0°$) but smaller than θ_2 ($= 206.6°$) under the conditions ($\theta_1 < \theta < \theta_2$: $45.0 < \theta < 206.6°$).

The behavior of θ, which depends on k via α, is as follows: θ becomes larger starting from θ_1 ($= 45.0°$) at (k, α) = (0, 1) to 90.0° at (−1, 0) in the first quadrant. It increases further to 180.0°, where (k, α) = (−2, −∞) in the fourth quadrant; $\theta = 180.0°$ is also satisfied by (k, α) = (−2, ∞). The value approaches a maximum at θ_2 ($= 206.6°$), where (k, α) = (−∞, 2.0) in the third quadrant. Namely, the acceptable range of θ in the plots is θ_1 ($= 45.0°$) $< \theta < \theta_2$ ($= 206.6°$), as mentioned above. Other ranges are unlikely since $H_b(\boldsymbol{r}_c) \geq H_b(\boldsymbol{r}_c) - V_b(\boldsymbol{r}_c)/2$ for $0.0° \leq \theta \leq \theta_1$ in the first quadrant, $270.0 \leq \theta \leq 360.0°$ in the second quadrant, and $225.0 \leq \theta \leq 270.0°$ in the third quadrant, together with $k \geq 0$ for $\theta_2 \leq \theta \leq 225.0°$ in the third quadrant. Figure 4 illustrates the acceptable range of θ in the plots, together with some typical values of θ at (k, α).

The helical stream in the plots of $H_b(\boldsymbol{r}_c)$ versus $H_b(\boldsymbol{r}_c) - V_b(\boldsymbol{r}_c)/2$ for weak to strong interactions must appear in the acceptable range of θ. The k controls the range and whole picture of the helical stream, since θ is determined by k via α. Behaviors of the AIM parameters, R, θ, θ_p, and κ_p, will be discussed next.

Behaviors of R, θ, θ_p, and κ_p in Relation to k. Figures 5−8 show the plots of the parameters, R, θ, θ_p, and κ_p, versus k, respectively. Plots of the AIM functions in Table 2 ($\rho_b(\boldsymbol{r}_c)$, $H_b(\boldsymbol{r}_c)$, and $H_b(\boldsymbol{r}_c) - V_b(\boldsymbol{r}_c)/2$) versus k are shown in Figures S2−S4 of the Supporting Information, respectively.[46]

R must be controlled both by k and $G_b(\boldsymbol{r}_c)$, as shown in eq 7. Therefore, the relation between R and k may not be simple. Figure 5 shows the plot of R versus $1/k$,[46] which is rather simple, however. The plot is analyzed for TB-MC, X_3^-, CT-TBP, and classical chemical bonds ($k \leq -1$), assuming the exponential

TABLE 2: Typical Ranges of $\rho_b(\boldsymbol{r}_c)$, $\nabla^2\rho_b(\boldsymbol{r}_c)$, $H_b(\boldsymbol{r}_c)$, and $H_b(\boldsymbol{r}_c) - V_b(\boldsymbol{r}_c)/2$ for Some Kinds of Interactions

interaction	$\rho_b(\boldsymbol{r}_c)^a$ (ea_o^{-3})	$\nabla^2\rho_b(\boldsymbol{r}_c)^b$ (ea_o^{-5})	$H_b(\boldsymbol{r}_c)^c$ (au)	$H_b(\boldsymbol{r}_c) - V_b(\boldsymbol{r}_c)/2^d$ (au)
vdW	$0.00 < \rho_{bc} < 0.01$	$0.00 < \nabla^2\rho_{bc} < 0.05$	$0 < H_{bc} < 0.003$	$0 < H_{vbc} < 0.007$
HBs	$0.01 < \rho_{bc} < 0.04$	$0.06 < \nabla^2\rho_{bc} < 0.12$	$-0.01 < H_{bc} < 0.003$	$0.007 < H_{vbc} < 0.02$
CT-MCs	$0.02 < \rho_{bc} < 0.07$	$0.06 < \nabla^2\rho_{bc} < 0.13$	$-0.02 < H_{bc} < 0$	$0.007 < H_{vbc} < 0.016$
X_3^-	$0.06 < \rho_{bc} < 0.10$	$0.05 < \nabla^2\rho_{bc} < 0.11$	$-0.04 < H_{bc} < -0.01$	$0.006 < H_{vbc} < 0.014$
CT-TBPs	$0.06 < \rho_{bc} < 0.12$	$0.0 < \nabla^2\rho_{bc} < 0.06$	$-0.06 < H_{bc} < -0.02$	$0 < H_{vbc} < 0.007$
Cov-w	$0.1 < \rho_{bc} < 0.2$	$-0.4 < \nabla^2\rho_{bc} < 0.0$	$-0.15 < H_{bc} < -0.04$	$-0.05 < H_{vbc} < 0$
Cov-s	$0.2 < \rho_{bc} < 0.5$	$-1.7 < \nabla^2\rho_{bc} < -0.4$	$-0.8 < H_{bc} < -0.15$	$-0.2 < H_{vbc} < -0.05$

[a] $\rho_b(\boldsymbol{r}_c) = \rho_{bc}$. [b] $\nabla^2\rho_b(\boldsymbol{r}_c) = \nabla^2\rho_{bc}$. [c] $H_b(\boldsymbol{r}_c) = H_{bc}$. [d] $H_b(\boldsymbol{r}_c) - V_b(\boldsymbol{r}_c)/2 = (\hbar^2/8m)\nabla^2\rho_b(\boldsymbol{r}_c) = H_{vbc}$.

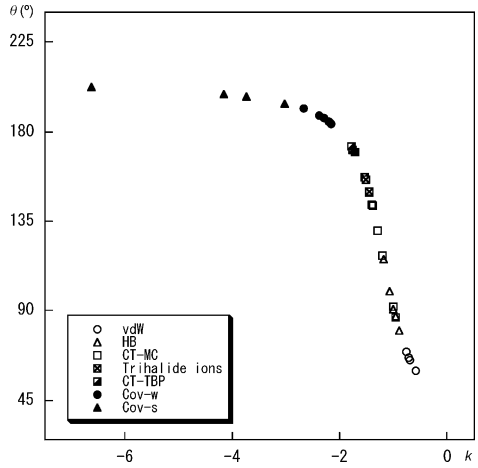

Figure 6. Plot of θ versus k.

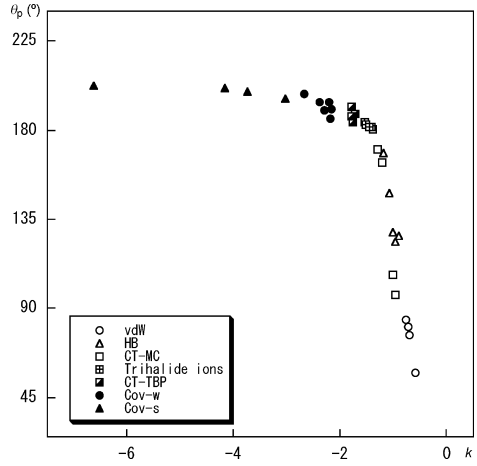

Figure 7. Plot of θ_p versus k.

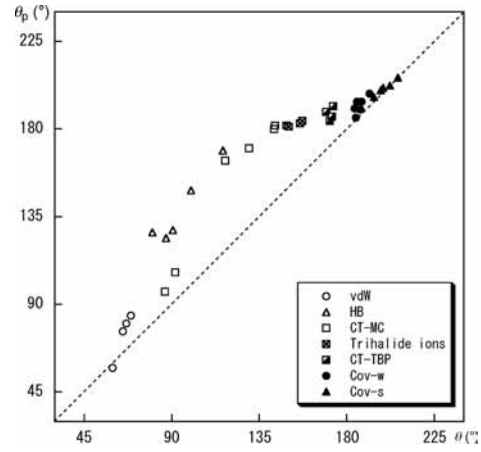

Figure 8. Plot of θ_p versus θ. The dotted line corresponds to $\theta_p = \theta$.

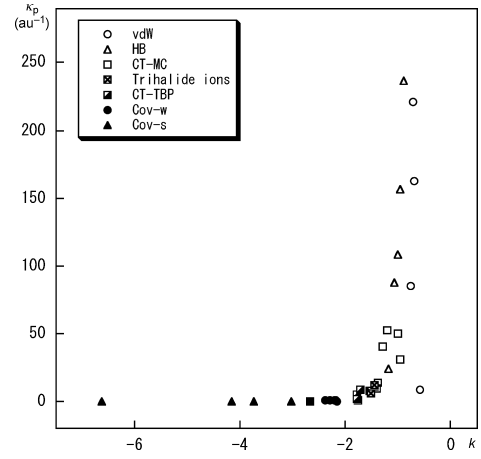

Figure 9. Plot of κ_p versus k.

function. The correlation is given in the figure, although data for Me_2O-X_2 (MC; X = Cl and Br), H_2, C_2H_4, and C_2H_2 are not contained. R grows rapidly for X_3^-, CT-TBP, and classical chemical bonds ($k \leq -2$). The range of $0 > k > -1$ corresponds to the pure CS interactions (Scheme 1). The vdW and HB interactions belong to the area. R for vdW and HB seem to be very small relative to the case with $k \leq -2$.

Figure 6 shows the plots of θ versus k; θ grows monotonically as k becomes more negative, which must be the reflection of the fact that θ is controlled only by k via α (eq 8). How does θ_p behave depending on k? Figure 7 displays the plot of θ_p versus k, which is similar to that of θ versus k. The resemblance between the two suggests that a common factor controls both θ and θ_p, which must be k. The correlation between θ and θ_p will clarify the nature in the plot of $H_b(\boldsymbol{r}_c)$ versus $H_b(\boldsymbol{r}_c) - V_b(\boldsymbol{r}_c)/2$. Figure 8 shows the plots of θ_p versus θ; θ_p is almost equal to θ for strong covalent bonds and for very weak vdW interactions such as He···H−F. On the other hand, $\theta_p > \theta$ for HB, CT-MC, X_3^-, and CT-TBP. Namely, the helical figure of the plots starts from near origin for very weak vdW interactions with $\theta_p \approx \theta$. Then, θ_p precedes along the helical stream by HB, CT-MC, X_3^-, and CT-TBP with $\theta_p > \theta$, as shown in Figure 8. The plots approach to the asymptotic line of $y = 2x$ ($x < 0$), where $\theta_p \approx \theta$ again at the final stage with Cov-s (see Figures 3 and 4). It is worthwhile to comment that θ determines the helical stream of the plot at the full-optimized structures ($w = 0$), whereas θ_p corresponds to the helical stream for each plot of an interaction, arising from the perturbation calculated with the fixed bond length with $w = (0)$, ± 0.1, and ± 0.2 in $r = r_o + wa_o$.

The curvature in the plots of $H_b(\boldsymbol{r}_c)$ versus $H_b(\boldsymbol{r}_c) - V_b(\boldsymbol{r}_c)/2$ must be the reflection of the nature of each interaction at BCP. The change in $H_b(\boldsymbol{r}_c)$ versus r should be different from that in $H_b(\boldsymbol{r}_c) - V_b(\boldsymbol{r}_c)/2$ versus r. The κ_p value will be large when $H_b(\boldsymbol{r}_c)$ or $H_b(\boldsymbol{r}_c) - V_b(\boldsymbol{r}_c)/2$ can be analyzed assuming the parabolic curve (versus r). The κ_p is small for very weak interactions as in He···H−F (vdW). The magnitude of k is small for the interaction, and κ_p increases as the vdW interaction becomes stronger with the heavier rare gas atoms. It reaches maximum at around the border area between Kr···HF (vdW) and NN···HF (HB) (around BP1) and decreases as the interaction becomes stronger. The κ_p grows larger again at around CT-MC (around BP2) (see Table 1). It decreases after the area and becomes negligibly small for the covalent bonds. It seems difficult to explain the behavior of κ_p from k. Figure 9 illustrates the behavior of κ_p versus k.

Tables 2 and 3 summarize the typical ranges of the AIM functions ($\rho_b(\boldsymbol{r}_c)$, $\nabla^2\rho_b(\boldsymbol{r}_c)$, $H_b(\boldsymbol{r}_c)$, and $H_b(\boldsymbol{r}_c) - V_b(\boldsymbol{r}_c)/2$) and the AIM parameters (k, R, θ, θ_p, and κ_p), respectively, for the specific types of interactions shown in Scheme 2. The values in Tables 2 and 3 are well separated for weak to strong interactions. Indeed, some ranges are overlapped, but the data for the interactions appear on the two-dimensional plane in the plots of $H_b(\boldsymbol{r}_c)$ versus $H_b(\boldsymbol{r}_c) - V_b(\boldsymbol{r}_c)/2$. Therefore, the separation of the data must be much better than that expected from Tables 2 and 3 (see Figure 3). The results demonstrate that the polar

TABLE 3: Typical Ranges of k, R, θ, θ_p, and κ_p for Some Kinds of Interactions

interaction	k	R (au)	θ^a (°)	$\theta_p{}^a$ (°)	κ_p (au^{-1})
vdW	$-0.8 < k$ (< 0)	$0 < R < 0.007$	$\theta_1 < \theta < 75$	$\theta_1 < \theta_p < 90$	$5 < \kappa_p < 230$
HB	$-1.5 < k < -0.8$	$0.007 < R < 0.013$	$75 < \theta < 120$	$120 < \theta_p < 170$	$20 < \kappa_p < 240$
CT-MC	$-1.8 < k < -1.0$	$0.01 < R < 0.02$	$85 < \theta < 145$	$160 < \theta_p < 185$	$5 < \kappa_p < 60$
X_3^-	$-1.7 < k < -1.2$	$0.02 < R < 0.04$	$145 < \theta < 160$	$180 < \theta_p < 185$	$5 < \kappa_p < 15$
CT-TBP	$-2.0 < k < -1.7$	$0.02 < R < 0.06$	$165 < \theta < 175$	$180 < \theta_p < 195$	$0 < \kappa_p < 10$
Cov-w	$-4.0 < k < -2.0$	$0.04 < R < 0.15$	$180 < \theta < 195$	$180 < \theta_p < 200$	$0 < \kappa_p < 1.5$
Cov-s	$-70^b < k \leq -3.0$	$0.15 < R < 0.8$	$190 < \theta < \theta_2$	$195 < \theta_p < \theta_2$	$0 < \kappa_p < 0.2$

[a] $\theta_1 = 45.0°$ and $\theta_2 = 206.6°$. [b] $k = -49.3$ for H_2 at the optimized distance (r_o) and -69.5 at $r = r_o - 0.2a_o$.

coordinate representation for the plots of $H_b(\boldsymbol{r}_c)$ versus $H_b(\boldsymbol{r}_c) - V_b(\boldsymbol{r}_c)/2$ is very useful to classify, evaluate, and understand weak to strong interactions. The k ($= V_b(\boldsymbol{r}_c)/G_b(\boldsymbol{r}_c)$) value is the key parameter of our treatment. The value is also well related to the SS ($k < -2.0$), pure CS ($k > -1.0$), and CS interactions with $\nabla^2\rho_b(\boldsymbol{r}_c) > 0$ and $H_b(\boldsymbol{r}_c) < 0$ ($-2.0 < k < -1.0$) (see Scheme 1).

We must be careful when the specific types of interactions are discussed based on the ranges of the AIM functions and parameters. The range of $H_b(\boldsymbol{r}_c)$ for CT-MC is predicted to be negative in Table 2 since the range is determined based on $Me_2Z\cdots X_2$ (Z = S, Se and X = Cl, Br). However, the range in $Me_2O\cdots X_2$ (X = Cl and Br) seems to extend over the positive area. The nature of the CT-MC interaction in $Me_2O\cdots X_2$ (X = Cl and Br) in this case could be understood as follows. The CT-MC interactions usually belong to the CS region with $H_b(\boldsymbol{r}_c) < 0$; however, the CT-MC interaction sometimes belongs to the pure CS interaction with $H_b(\boldsymbol{r}_c) > 0$, such as the case of $Me_2O\cdots X_2$ (X = Cl and Br). Interactions in $Me_2O\cdots X_2$ (X = Cl and Br) must contain the nature of HB, judging from the AIM functions and parameters in Table 2. Electrons of the usual CT-MC interactions are stabilized at BCP, whereas those in $Me_2O\cdots X_2$ (X = Cl and Br) would be destabilized at BCP. Namely, the range of an (formal) interaction sometimes does not correspond to the nature of the typical interaction. It is worthwhile to comment that the nature of an interaction can be discussed independently based on the AIM parameters and functions, irrespective of the typical range of the interaction (cf: Figure 2). The range should change depending on the species being employed for the determination.

Conclusion

The polar coordinate (R, θ) representation of the plot for $H_b(\boldsymbol{r}_c)$ versus $(\hbar^2/8m)\nabla^2\rho_b(\boldsymbol{r}_c)$ ($= H_b(\boldsymbol{r}_c) - V_b(\boldsymbol{r}_c)/2$) is demonstrated to be useful to classify, evaluate, and understand the nature of weak to strong interactions in a unified way and in more detail. The plots construct a helical stream as a whole starting from the origin ($H_b(\boldsymbol{r}_c) = H_b(\boldsymbol{r}_c) - V_b(\boldsymbol{r}_c)/2 = 0$), and both $H_b(\boldsymbol{r}_c)$ and $H_b(\boldsymbol{r}_c) - V_b(\boldsymbol{r}_c)/2$ increase, and then, the plots turn to the right, drawing a helical figure. The helical nature of the plots is controlled by the relative magnitudes of $G_b(\boldsymbol{r}_c)$ and $V_b(\boldsymbol{r}_c)$ ($k = V_b(\boldsymbol{r}_c)/G_b(\boldsymbol{r}_c)$). R in (R, θ) corresponds to the energy for an interaction at BCP in the ($H_b(\boldsymbol{r}_c) - V_b(\boldsymbol{r}_c)/2$, $H_b(\boldsymbol{r}_c)$) plane relative to that without any interaction. The helical figure is expressed by θ measured from the y-axis. The acceptable θ value is shown to be $45.0 < \theta < 206.6°$. Each plot of $H_b(\boldsymbol{r}_c)$ versus $H_b(\boldsymbol{r}_c) - V_b(\boldsymbol{r}_c)/2$ for an interaction gives a curve, which must be the reflection of the nature of the interaction at BCP. The curve is analyzed by θ_p and κ_p; θ_p corresponds to the tangent line measured from the y-direction, and κ_p is the curvature of the correlation for the plot. The k value must be the key parameter of the treatment. The AIM parameters (k, R, θ, θ_p, and κ_p) are well separated by the interaction groups shown in Scheme 2. The polar coordinate representation for the plots of $H_b(\boldsymbol{r}_c)$ versus $H_b(\boldsymbol{r}_c) - V_b(\boldsymbol{r}_c)/2$ enables us to classify, evaluate, and understand weak to strong interactions. The interaction map in chemistry could be developed by applying the method to the wide range of weak to strong interactions. The treatment will also help us to understand the nature of the interactions in a unified way.

Investigations for the applications of the proposed method are in progress. The results will be reported elsewhere.

Acknowledgment. This work was partially supported by a Grant-in-Aid for Scientific Research (Grants 16550038, 19550041, and 20550042) from the Ministry of Education, Culture, Sports, Science, and Technology, Japan.

Supporting Information Available: AIM Parameters for examined molecules and adducts; plots of $H_b(\boldsymbol{r}_c)$ and $H_b(\boldsymbol{r}_c) - V_b(\boldsymbol{r}_c)/2$ versus w in $r = r_o + wa_o$ for Cl_3^- and Br_3^-, where r_o and a_o stand for the full-optimized bond distance and the Bohr radius, respectively; plots of $\rho_b(\boldsymbol{r}_c)$, $H_b(\boldsymbol{r}_c)$, and $H_b(\boldsymbol{r}_c) - V_b(\boldsymbol{r}_c)/2$ versus $1/k$ for the species in Scheme 2; optimized structures given by Cartesian coordinates for examined molecules and adducts. This material is available free of charge via the Internet at http://pubs.acs.org.

References and Notes

(1) (a) *Atoms in Molecules. A Quantum Theory*: Bader, R. F. W., Ed.; Oxford University Press: Oxford, U.K., 1990. (b) Matta, C. F.; Boyd, R. J. *An Introduction to the Quantum Theory of Atoms in Molecules In The Quantum Theory of Atoms in Molecules: From Solid State to DNA and Drug Design*; Matta, C. F., Boyd, R. J., Eds.; Wiley-VCH: Weinheim, Germany, 2007; Chapter 1.

(2) (a) Bader, R. F. W.; Slee, T. S.; Cremer, D.; Kraka, E. *J. Am. Chem. Soc.* **1983**, *105*, 5061–5068. (b) Bader, R. F. W. *Chem. Rev.* **1991**, *91*, 893–928. (c) Bader, R. F. W. *J. Phys. Chem. A* **1998**, *102*, 7314–7323. (d) Biegler-König, F.; Bader, R. F. W.; Tang, T. H. *J. Comput. Chem.* **1982**, *3*, 317–328. (e) Bader, R. F. W. *Acc. Chem. Res.* **1985**, *18*, 9–15. (f) Tang, T. H.; Bader, R. F. W.; MacDougall, P. *Inorg. Chem.* **1985**, *24*, 2047–2053. (g) Biegler-König, F.; Schönbohm, J.; Bayles, D. *J. Comput. Chem.* **2001**, *22*, 545–559. (h) Biegler-König, F.; Schönbohm, J. *J. Comput. Chem.* **2002**, *23*, 1489–1494.

(3) Molina, J.; Dobado, J. A. *Theor. Chem. Acc.* **2001**, *105*, 328–337.

(4) Dobado, J. A.; Martinez-Garcia, H.; Molina, J.; Sundberg, M. R. *J. Am. Chem. Soc.* **2000**, *122*, 1144–1149.

(5) Yamashita, M.; Yamamoto, Y.; Akiba, K.-y.; Hashizume, D.; Iwasaki, F.; Takagi, N.; Nagase, S. *J. Am. Chem. Soc.* **2005**, *127*, 4354–4371.

(6) Ignatov, S. K.; Rees, N. H.; Tyrrell, B. R.; Dubberley, S. R.; Razuvaev, A. G.; Mountford, P.; Nikonov, G. I. *Chem.—Eur. J.* **2004**, *10*, 4991–4999.

(7) Muchall, H. M. *ARKIVOC* **2001**, *7*, 82–86.

(8) Tripathi, S. K.; Patel, U.; Roy, D.; Sunoj, R. B.; Singh, H. B.; Wolmershäuser, G.; Butcher, R. J. *J. Org. Chem.* **2005**, *70*, 9237–9247.

(9) Boyd, R. J.; Choi, S. C. *Chem. Phys. Lett.* **1986**, *129*, 62–65.

(10) Carroll, M. T.; Bader, R. F. W. *Mol. Phys.* **1988**, *65*, 695–722.

(11) Espinosa, E.; Molins, E.; Lecomte, C. *Chem. Phys. Lett.* **1998**, *285*, 170–173.

(12) Grabowski, S. J. *J. Phys. Chem. A* **2001**, *105*, 10739–10746.
(13) (a) Espinosa, E.; Alkorta, I.; Elguero, J.; Molins, E. *J. Chem. Phys.* **2002**, *117*, 5529–5542. (b) Rozas, I.; Alkorta, I.; Elguero, J. *J. Am. Chem. Soc.* **2000**, *122*, 11154–11161.
(14) Domagala, M.; Grabowski, S.; Urbaniak, K.; Mloston, G. *J. Phys. Chem. A* **2003**, *107*, 2730–2736.
(15) Grabowski, S.; Sokalski, W. A.; Leszczynski, J. *J. Phys. Chem. A* **2005**, *109*, 4331–4341.
(16) Domagala, M.; Grabowski, S. *J. Phys. Chem. A* **2005**, *109*, 5683–5688.
(17) The bond order (BO), which corresponds to the strength of a chemical bond, is correlated to $\rho_b(\boldsymbol{r}_c)$ by the form shown below, where A and B are constants which depend on the nature of the bonded atoms;[1b] BO $= \exp[A(\rho_b(\boldsymbol{r}_c) - B)]$.
(18) Nakanishi, W.; Nakamoto, T.; Hayashi, S.; Sasamori, T.; Tokitoh, N. *Chem.—Eur. J.* **2007**, *13*, 255–268.
(19) (a) *Molecular Interactions. From van der Waals to Strongly Bound Complexes*: Scheiner, S., Ed.; Wiley: New York, 1997. (b) Asmus, K. D. *Acc. Chem. Res.* **1979**, *12*, 436–442. (c) Musker, W. K. *Acc. Chem. Res.* **1980**, *13*, 200–206. (d) Kucsman, A.; Kapovits, I. Non-Bonded Sulfur-Oxygen Interaction in Organic Sulfur Compounds. In *Organic Sulfur Compounds in Organic Sulfur Chemistry: Theoretical and Experimental Advances*; Bernardi, F., Csizmadia, I. G., Mangini, A., Eds.; Elsevier: Amsterdam, The Netherlands, 1985; Chapter 4.
(20) *Chemistry of Hypervalent Compounds*; Akiba, K.-y., Ed.; Wiley-VCH: New York, 1999.
(21) Nakanishi, W. *Hypervalent Chalcogen Compounds In Handbook of Chalcogen Chemistry: New Perspectives in Sulfur, Selenium and Tellurium*; Devillanova, F. A., Ed.; Royal Society of Chemistry: Cambridge, U.K., 2006; Chapter 10.3, pp 644−668.
(22) (a) Nakanishi, W. *Chem. Lett.* **1993**, 2121–2122. (b) Nakanishi, W.; Hayashi, S.; Toyota, S. *Chem. Commun.* **1996**, 371–372. (c) Nakanishi, W.; Hayashi, S.; Yamaguchi, H. *Chem. Lett.* **1996**, 947–948. (d) Nakanishi, W.; Hayashi, S.; Sakaue, A.; Ono, G.; Kawada, Y. *J. Am. Chem. Soc.* **1998**, *120*, 3635–3640. (e) Nakanishi, W.; Hayashi, S.; Toyota, S. *J. Org. Chem.* **1998**, *63*, 8790–8800. (f) Hayashi, S.; Nakanishi, W. *J. Org. Chem.* **1999**, *64*, 6688–6696. (g) Nakanishi, W.; Hayashi, S.; Uehara, T. *J. Phys. Chem. A,* **1999**, *103*, 9906–9912. (h) Nakanishi, W.; Hayashi, S. *J. Org. Chem.* **2002**, *67*, 38–48. (i) Hayashi, S.; Wada, H.; Ueno, T.; Nakanishi, W. *J. Org. Chem.* **2006**, *71*, 5574–5585.
(23) (a) Nakanishi, W.; Hayashi, S.; Kihara, H. *J. Org. Chem.* **1999**, *64*, 2630–2637. (b) Nakanishi, W.; Hayashi, S.; Uehara, T. *Eur. J. Org. Chem.* **2001**, 3933–3943.
(24) Rosenfield, R. E.; Parthasarathy, R., Jr.; Dunitz, J. D. *J. Am. Chem. Soc.* **1977**, *99*, 4860–4862.
(25) *The Weak Hydrogen Bond in Structural Chemistry and Biology*, International Union of Crystallography Monographs on Crystallography; Desiraju, G. R., Steiner, T. Eds.; Oxford University Press: New York, 1999.
(26) (a) Steiner, T. *Angew. Chem.* **2002**, *114*, 50–80. (b) Steiner, T. *Angew. Chem., Int. Ed.* **2002**, *41*, 48–76.
(27) Bleiholder, C.; Werz, D. B.; Köppel, H.; Gleiter, R. *J. Am. Chem. Soc.* **2006**, *128*, 2666–2674. Bleiholder, C.; Gleiter, R.; Werz, D. B.; Köppel, H. *Inorg. Chem.* **2007**, *46*, 2249–2260.
(28) Rêthorê, C.; Madalan, A.; Fourmiguê, M.; Canadell, E.; Lopes, E. B.; Almeida, M.; Clêrac, R.; Avarvari, N. *New J. Chem.* **2007**, *31*, 1468–1483.
(29) (a) Suzuki, T.; Fujii, H.; Yamashita, Y.; Kabuto, C.; Tanaka, S.; Harasawa, M.; Mukai, T.; Miyashi, T. *J. Am. Chem. Soc.* **1992**, *114*, 3034–3043. (b) Turbiez, M.; Frêre, P.; Allain, M.; Videlot, C.; Ackermann, J.; Roncali, J. *Chem.—Eur. J.* **2005**, *11*, 3742–3752. (c) Cozzolino, A. F.; Vargas-Baca, I.; Mansour, S.; Mahmoudkhani, A. H. *J. Am. Chem. Soc.* **2005**, *127*, 3184–3190.
(30) Lippolis, V.; Isaia, F. Charge Transfer (C.-T.) Adducts and Related Compounds. In *Handbook of Chalcogen Chemistry: New Perspectives in Sulfur, Selenium and Tellurium*; Devillanova, F. A., Ed.; Royal Society of Chemistry: Cambridge, U.K., 2006; Chapter 8.2, pp 477−499. (b) Rêthorê, C.; Fourmiguê, M.; Avarvari, N. *Chem. Commun.* **2004**, 1384–1385. (c) Rêthorê, C.; Fourmiguê, M.; Avarvari, N. *Tetrahedron* **2005**, *61*, 10935–10942. (d) Rêthorê, C.; Avarvari, N.; Canadell, E.; Auban-Senzier, P.; Fourmiguê, M. *J. Am. Chem. Soc.* **2005**, *127*, 5748–5749.
(31) (a) Desiraju, G. R. *Angew. Chem.* **1995**, *107*, 2541–2558. (b) Desiraju, G. R. *Angew. Chem., Int. Ed. Engl.* **1995**, *34*, 2311–2327.
(32) (a) Burling, F. T.; Goldstein, B. M. *J. Am. Chem. Soc.* **1992**, *114*, 2313–2320. (b) Nagao, Y.; Hirata, T.; Goto, S.; Sano, S.; Kakehi, A.; Iizuka, K.; Shiro, M. *J. Am. Chem. Soc.* **1998**, *120*, 3104–3110. (c) Wu, S.; Greer, A. *J. Org. Chem.* **2000**, *65*, 4883–4887. (d) Nagao, Y.; Iimori, H.; Goto, S.; Hirata, T.; Sano, S.; Chuman, H.; Shiro, M. *Tetrahedron Lett.* **2002**, *43*, 1709–1712. (e) Meyer, E.; Joussef, A. C.; Gallardo, H.; Bortoluzzi, A. J.; Longo, R. L. *Tetrahedron* **2003**, *59*, 10187–10193. (f) Nagao, Y.; Honjo, T.; Iimori, H.; Goto, S.; Sano, S.; Shiro, M.; Yamaguchi, K.; Sei, Y. *Tetrahedron Lett.* **2004**, *45*, 8757–8761.
(33) (a) Taylor, J. C.; Markham, G. D. *J. Biol. Chem.* **1999**, *274*, 32909–32914. (b) Brandt, W.; Golbraikh, A.; Täger, M.; Lendeckel, U. *Eur. J. Biochem.* **1999**, *261*, 89–97.
(34) Nakanishi, W.; Hayashi, S.; Narahara, K. *J. Phys. Chem. A* **2008**, *112*, 13593–13599.
(35) Methyl-substituted compounds are used to calculate the AIM parameters in order to compare the data to those under the experimental conditions more easily.
(36) For van der Waals interactions, see also: (a) Dessent, C. E. H.; Müller-Dethlefs, K. *Chem. Rev.* **2000**, *100*, 3999–4021. (b) Wormer, P. E. S.; van der Avoird, A. *Chem. Rev.* **2000**, *100*, 4109–4143.
(37) For hydrogen bonds, see: (a) Espinosa, E.; Souhassou, M.; Lachekar, H.; Lecomte, C. *Acta Crystallogr., Sect. B* **1999**, *55*, 563–572. (b) Espinosa, E.; Lecomte, C.; Molins, E. *Chem. Phys. Lett.* **1999**, *300*, 745–748. (c) Espinosa, E.; Alkorta, I.; Rozas, I.; Elguero, J.; Molins, E. *Chem. Phys. Lett.* **2001**, *336*, 457–461. (d) Gatti, C.; Bertini, L. *Acta Crystallogr., Sect. A* **2004**, *60*, 438–449.
(38) Frisch, M. J.; Trucks, G. W.; Schlegel, H. B.; Scuseria, G. E.; Robb, M. A.; Cheeseman, J. R.; Montgomery, J. A., Jr.; Vreven, T.; Kudin, K. N.; Burant, J. C.; Millam, J. M.; Iyengar, S. S.; Tomasi, J.; Barone, V.; Mennucci, B.; Cossi, M.; Scalmani, G.; Rega, N.; Petersson, G. A.; Nakatsuji, H.; Hada, M.; Ehara, M.; Toyota, K.; Fukuda, R.; Hasegawa, J.; Ishida, M.; Nakajima, T.; Honda, Y.; Kitao, O.; Nakai, H.; Klene, M.; Li, X.; Knox, J. E.; Hratchian, H. P.; Cross, J. B.; Bakken, V.; Adamo, C.; Jaramillo, J.; Gomperts, R.; Stratmann, R. E.; Yazyev, O.; Austin, A. J.; Cammi, R.; Pomelli, C.; Ochterski, J. W.; Ayala, P. Y.; Morokuma, K.; Voth, G. A.; Salvador, P.; Dannenberg, J. J.; Zakrzewski, V. G.; Dapprich, S.; Daniels, A. D.; Strain, M. C.; Farkas, O.; Malick, D. K.; Rabuck, A. D.; Raghavachari, K.; Foresman, J. B.; Ortiz, J. V.; Cui, Q.; Baboul, A. G.; Clifford, S.; Cioslowski, J.; Stefanov, B. B.; Liu, G.; Liashenko, A.; Piskorz, P.; Komaromi, I.; Martin, R. L.; Fox, D. J.; Keith, T.; Al-Laham, M. A.; Peng, C. Y.; Nanayakkara, A.; Challacombe, M.; Gill, P. M. W.; Johnson, B.; Chen, W.; Wong, M. W.; Gonzalez, C.; Pople, J. A. *Gaussian 03*, revision D.02; Gaussian, Inc.: Wallingford, CT, 2004.
(39) (a) Møller, C.; Plesset, M. S. *Phys. Rev.* **1934**, *46*, 618–622. (b) Gauss, J. *J. Chem. Phys.* **1993**, *99*, 3629–3643. (c) Gauss, J. *Ber. Bunsen-Ges. Phys. Chem.* **1995**, *99*, 1001–1008.
(40) The molecular graph is known as the collection of bond paths linking the nuclei of bonded atoms with the associated critical points in the equilibrium geometry. The molecular graph provides an unambiguous definition of the "molecular structure" and can thus be used to locate changes in structure along a reaction path.[1]
(41) In a nonequilibrium geometry discussed in this treatment, lines of maximum electron density linking the nuclei are known as "atomic interaction lines" because these may or may not persist when the geometry is energy-minimized, that is, optimized.[1] However, the trends could be discussed as the extension of those for the optimized structures in our treatment since the geometries converge to the optimized ones when started from the given nonequilibrium ones.
(42) The bond orders become 1.50 and 0.67 times larger than the initial value if they are calculated at $0.2a_o$ shorter and longer distances from the initial length, respectively.
(43) Regardless of the treatment, as in ref 41, we will call the AIM functions and/or parameters at $r_o - 0.2a_o < r < r_o + 0.2a_o$ similar to the case of the equilibrium geometry here.
(44) The AIM 2000 program (version 2.0) was employed to analyze and visualize atoms-in-molecules: Biegler-König, F. *J. Comput. Chem.* **2000**, *21*, 1040−1048; see also ref 2g.
(45) Equations 8 and 9 correspond to eqs R1 and R2, respectively.

$$\tan(90 - \theta) = H_b(\boldsymbol{r}_c)/(\hbar^2/8m)\nabla^2\rho_b(\boldsymbol{r}_c) = H_b(\boldsymbol{r}_c)/(H_b(\boldsymbol{r}_c) - V_b(\boldsymbol{r}_c)/2) \quad \text{(R1)}$$

$$\tan(90 - \theta_p) = dH_b(\boldsymbol{r}_c)/d(H_b(\boldsymbol{r}_c) - V_b(\boldsymbol{r}_c)/2) = [dH_b(\boldsymbol{r}_c)/dr]_{r=r_o}/[H_b(\boldsymbol{r}_c) - (1/2)V_b(\boldsymbol{r}_c)/dr]_{r=r_o} \quad \text{(R2)}$$

(46) Plots versus $1/k$ are employed since some k values are very small.

JP903622A